IOP PUBLISHING JOURNAL OF PHYSICS D: APPLIED PHYSICS

J. Phys. D: Appl. Phys. **41** (2008) 035202 (8pp) doi:10.1088/0022-3727/41/3/035202

Electrical and plasma characteristics of a quasi-steady sliding discharge

R Sosa[1], H Kelly[2], D Grondona[2], A Márquez[2], V Lago[3] and G Artana[1]

[1] Laboratorio de Fluidodinámica, Universidad de Buenos Aires, Av. Paseo Colon 850, C1063ACV, Cdad. de Buenos Aires, Argentina

[2] Instituto de Física del Plasma, CONICET-Departamento de Física, FCEN, Universidad de Buenos Aires, Cdad. Universitaria, Pab. I, C1428EHA, Cdad. de Buenos Aires, Argentina

[3] CNRS, Laboratoire d'Aérothermique, 1C Av. de la Recherche Scientifique, 45071 Orléans, France

E-mail: rsosa@fi.uba.ar

Received 11 September 2007, in final form 1 November 2007
Published 9 January 2008
Online at stacks.iop.org/JPhysD/41/035202

Abstract

A quasi-steady sliding discharge at atmospheric pressure is generated by combining a surface dielectric barrier together with a DC corona discharge in a three-electrode geometry. The discharge extends along the whole side-length of the electrodes (150 mm) and covers the full inter-electrode gap (30 mm). It is found that this discharge is composed of repetitive streamers that are uniformly distributed along the whole electrode length and that propagate along the inter-electrode gap with an average velocity of $\sim 2 \times 10^7$ cm s^{-1}, and with an average electric field of ~ 120 kV cm^{-1} and a total particle number of $\sim 5 \times 10^8$ at the streamer head. Assuming that the electron distribution function reaches an equilibrium value with the electric field, an electron temperature of 9 eV at the streamer head is obtained. The streamer frequency is around 5×10^4 Hz for a well-developed sliding discharge regime, and the time-averaged electron density amounts to 1.5×10^7 cm^{-3}.

(Some figures in this article are in colour only in the electronic version)

1. Introduction

Currently, there is remarkable interest in developing stationary low-power plasma sources at high pressure. Their main advantage is that a non-equilibrium plasma state in atmospheric pressure gases can be established in an economical and reliable way. This plasma is characterized by a low enough ionization degree, so the electric energy delivered by the external power source goes into the heating of a small number of electrons, while the heavy particles (ions and molecules) remain relatively cold. Up to now, non-equilibrium plasma discharges have been employed in several important applications, including ozone production, surface modification of polymers, excitation of CO_2 lasers, pollution control and more recently plasma display panels for flat television screens (see [1] and references therein). Although most applications of these plasmas involve volume discharges, surface discharges have also been employed as ultraviolet sources for lasers (see [2] and references therein). Surface discharges are also being actively investigated in aerodynamic applications, that is, the control of the boundary layer of aerodynamic moving objects by using the 'electric wind' they produce or by a modification of some physical properties of the gas (viscosity, density) in the vicinity of the surface [3–6].

Despite numerous advances in applications of surface discharges to practical devices, many of the basic physical processes are not well understood. This is due to the use of different power sources (DC, AC or pulsed), different electrode geometries and different gas pressures and gas mixtures, which lead to vastly varied discharge modes (including filamentary, regularly patterned or diffuse discharges [7]).

This work describes an investigation of an atmospheric pressure surface discharge generated by the combined action of DC and AC power sources applied over three electrodes, with the goal of addressing its electrical and plasma characteristics.

2. Experimental set-up

The schematic of the experimental set-up is shown in figure 1. The electrode arrangement consisted of two flat aluminium foils air exposed and flush mounted on a dielectric surface

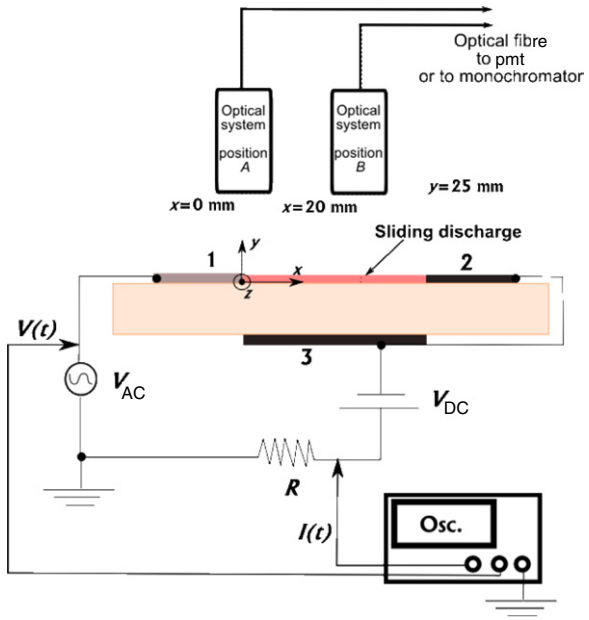

Figure 1. Experimental set-up.

(electrodes 1 and 2) and a third one located at the opposite side of that surface (electrode 3).

A variable DC power supply (V_{DC} in the range -6 to -20 kV, 10 W) biased negatively both electrodes 2 and 3. Another variable AC sine voltage power supply (frequency: $f = 9.7$ kHz, zero mean value; peak voltage V_{AC} in the range 6–14 kV) was applied to electrode 1. The AC power supply consisted of a function generator coupled to an audio amplifier (of 150 W) that fed a high voltage transformer coil [8].

In practice, the application of only the AC power source produced a surface dielectric barrier discharge (SDBD) between electrodes 1 and 3, while the combination of the AC and DC power sources produced (under certain values of the operating parameters) a sliding plasma sheet between electrodes 1 and 2, which covered the whole inter-electrode gap. A scheme of the sliding discharge path is indicated in figure 1.

The electrode dimensions were 50 μm thickness, 150 mm length (in the z direction, see figure 1) and different widths (50 mm for electrodes 1 and 2 and 30 mm for electrode 3). The flat dielectric plate was made of poly-methyl methacrylate (PMMA) with a thickness of 4 mm. The inter-electrode gap between electrodes 1 and 2 was 30 mm.

The electric current flowing in the system, $I(t)$, was measured with a shunt resistance, $R = 1\,\text{k}\Omega$, connected to an oscilloscope with 60 MHz of analogical bandwidth and 1 Gs s^{-1} of sampling rate. The AC voltage applied to electrode 1, $V(t)$, was measured with a HV probe (1000×/3.0 pF/100 MΩ).

The light emitted from the discharge was detected by an optical system consisting of a converging lens and a quartz optical fibre coupled to either a photo-multiplier tube (pmt) or the entrance slit of a monochromator. The pmt was able to detect light in the wavelength range 185–650 nm, with a response time and a transit time of 2.2 ns and 22 ns, respectively. The focal distance of the converging lens was $F = 5$ cm and the optical fibre radius was $r_{of} = 1$ mm. The field of view of the optical system was a slit of 20 mm × 5 mm in the z and x directions, respectively (see figure 1). The converging lens was located at two different positions: $x = 0$, $y = 25$ mm, $z = 0$ mm (position A, focusing on the SDBD)and $x = 20$ mm, $y = 25$ mm, $z = 0$ mm (position B, focusing on the sliding discharge) see figure 1. The origin of the z coordinate was chosen at the middle of the electrodes.

The discharge optical emission of the spectral bands corresponding to the 0–0 transition of the second positive system of $N_2(\lambda = 337.1\,\text{nm})$ and the first negative system of $N_2^+(\lambda = 391.4\,\text{nm})$ was also measured. The light emitted from the plasma sheet was detected by a monochromator SOPRA F1500 of the Ebert–Fastie-type with a focal length of 1500 mm and a diffraction grating of 1800 grooves mm^{-1}. The detector was an intensified OMA (Princeton Instruments IRY 1024) with a displayed optical window of 8.5 nm. The absolute detector sensitivity (S) was experimentally determined by obtaining the detector response (in number of counts) using a laser (with known power emission) as the light source and by further correcting the wavelength difference between the laser light and the registered wavelength (using an available sensitive wavelength response curve for the OMA detector). The sensitivity value resulted in $S = (4.3 \pm 0.5) \times 10^{-10}$ J/count (i.e. joules per detector count).

3. Results

3.1. Morphology of the discharge

The quasi-steady sliding discharge resulted from a combination of two single discharges (AC and DC) that presented individual thresholds for its respective voltage values (in this work the AC voltage value will be characterized by its peak value, unless otherwise stated).

The AC discharge, generated by applying AC voltage on electrode 1, was a SDBD that began to produce current pulses at a threshold peak value $V_{SDBD} = 5$ kV for the electrode geometry employed in this work. The presence of these pulses was accompanied by a faint violet–bluish light extending up to ∼1 cm in the x direction over the insulator surface.

The DC discharge between electrodes 1 and 2 (with electrode 1 grounded and 2 negatively biased) was an almost dark negative corona discharge that provided negative charges drifting from 2 to 1, thus being a source of negative charges distributed in the whole inter-electrode space and at the insulator surface. The corona was always ignited for the V_{DC} range of values investigated, and with a steady current varying in the range 30–300 μA for V_{DC} in the range -6 to -20 kV.

The sequence of photographs presented in figure 2 gives an example of the result of combining both discharges. The images corresponded to an exposure time of 2 s, with a fixed value of $V_{DC} = -16$ kV, and for increasing values of V_{AC}. The first image (figure 2(*a*)) corresponded to a V_{AC} value below the SDBD threshold, and it can be seen that the discharge presented relatively large active points oddly distributed along electrode 1. The discharge in this situation was noisy and unstable, with a high probability to spark transition. As

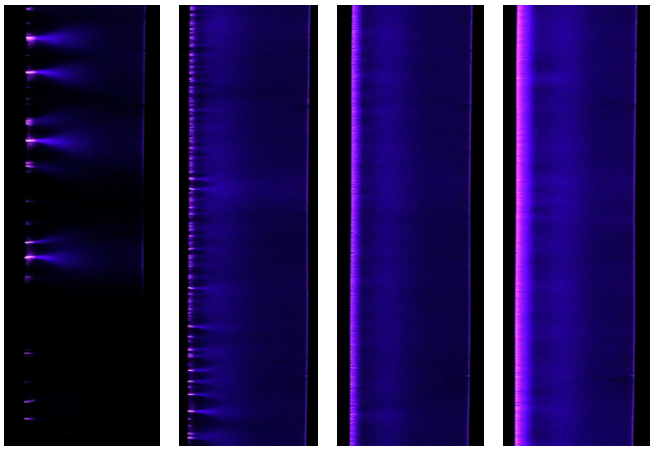

Figure 2. Discharge morphology. The pictures are top viewed with electrode 1 at the left and electrode 2 at the right; exposure time 2 s, $V_{DC} = -16$ kV. (*a*) $V_{AC} = 4.8$ kV; (*b*) $V_{AC} = 5.2$ kV; (*c*) $V_{AC} = 7.2$ kV; (*d*) $V_{AC} = 10.2$ kV.

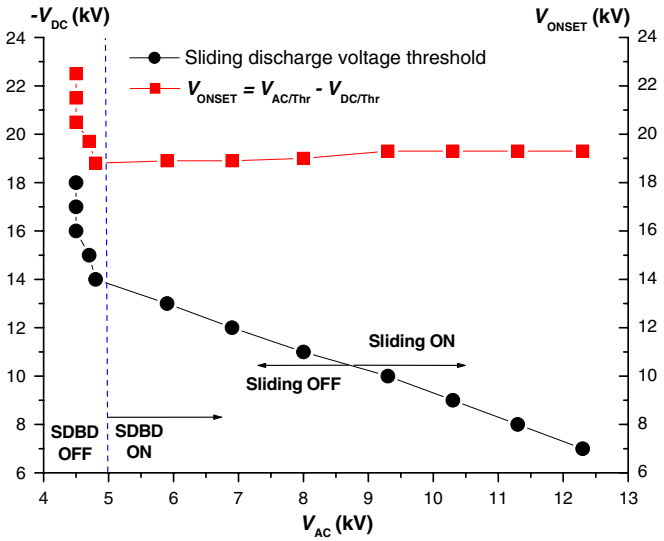

Figure 3. Voltage threshold values for the SDBD and sliding discharges.

long as V_{AC} was increased over the V_{SDBD} value, the active points reduced in size and their number became larger (see figures 2(*b*) and (*c*)). For sufficiently high V_{AC} values, the discharge showed a large amount of active points evenly distributed over the whole electrode side-length. In this situation, the discharge was almost silent and stable, with a bluish light covering the whole inter-electrode space, and could be sustained for large time periods (quasi-steady sliding discharge, see figure 2(*d*)).

In figure 3 a plot of V_{DC} versus V_{AC} is presented which allows identifying the different voltage threshold values where active luminous dots on electrode 1 are seen (solid circular points in the figure). The vertical dashed line (corresponding to $V_{SDBD} = 5$ kV) delimits the regions where the SDBD discharge is 'on' or 'off', so the solid circular points located to the left of this line represent situations of unstable discharges (as was shown in figure 2(*a*)). The region located at the right of the vertical dashed line and above the solid line joining the circles corresponds to the quasi-steady sliding discharge regime. Also, the quantity $V_{onset} = -V_{DC} + V_{AC}$ is included where the AC and DC voltage values correspond to the solid circular points of figure 3. Note that V_{onset} remains almost constant in the region where the quasi-steady sliding discharge is developed. The sequence of images presented in figure 2 corresponds to a displacement along the horizontal line passing through $V_{DC} = -16$ kV in figure 3.

It is interesting to note that for a relatively low fixed value of $-V_{DC}$ (in practice, smaller than 13 kV, a value that is not sufficient to produce a visible light pattern without the presence of the SDBD for our discharge geometry), an increase in the V_{AC} value produced a transition to the quasi-steady sliding discharge somewhat different from that presented in figure 2. This is shown in figure 4, where detailed images of the discharge with a large exposure time (8 s) around this transition are presented. The V_{DC} value was -10 kV in this case, corresponding to $V_{AC} = 9.4$ kV (see figure 3). It can be seen from figure 4(*a*) that below the sliding threshold ($V_{AC} = 9$ kV) only the light corresponding to the SDBD is

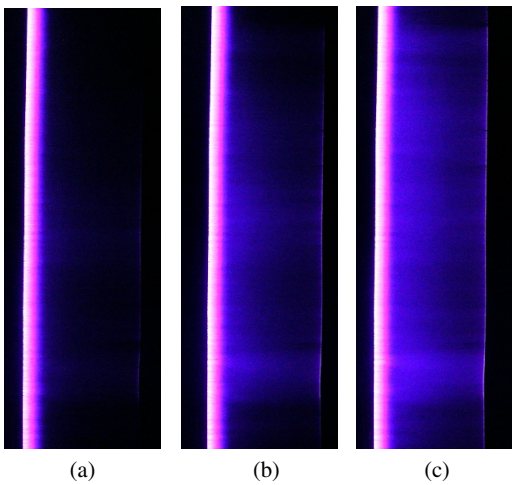

Figure 4. Sequence of pictures showing the establishment of the sliding discharge for increasing values of V_{AC}. Exposure time: 8 s. $V_{DC} = -10$ kV. (*a*) $V_{AC} = 9$ kV; (*b*) $V_{AC} = 9.4$ kV; (*c*) $V_{AC} = 9.7$ kV.

present, while for larger V_{AC} values the sliding discharge began to fill the whole inter-electrode gap extending in the z and x directions. In practice, this way of producing the quasi-steady sliding discharge is preferable, because there is no sparking risk in this case.

3.2. Electrical and optical characteristics of the discharge

In figure 5 the waveforms corresponding to $I(t)$, $V(t)$ and the pmt output signal, $V_{ph}(t)$, are presented for a completely developed sliding discharge situation ($V_{DC} = -14$ kV and $V_{AC} = 12.8$ kV).

Figure 5(*a*) corresponded to the optical system in position A (that is, 'seeing' the SDBD, see figure 1), while in figure 5(*b*) the optical system was in position B ('seeing' the sliding discharge but with the SDBD outside the field of view). It can be seen from figure 5(*a*) that the purely alternating reactive current component of the circuit is modified by the

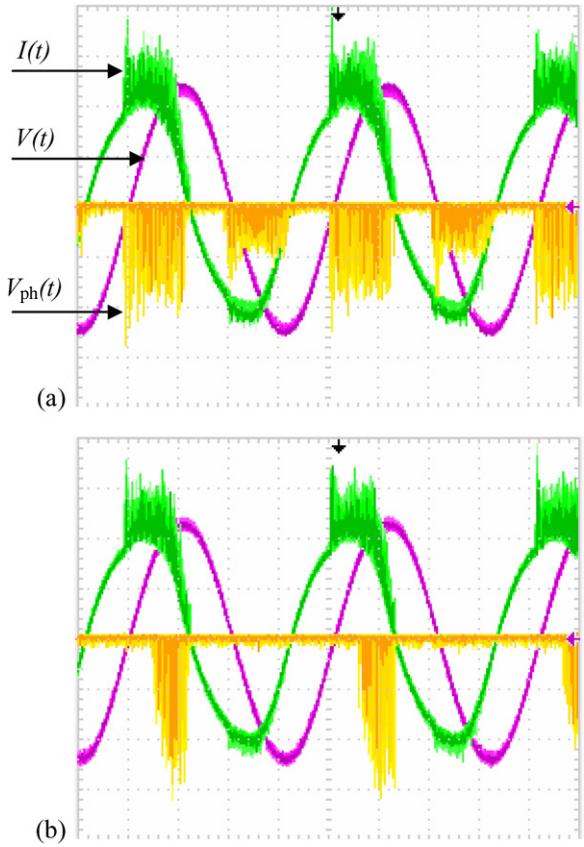

Figure 5. Waveforms of $I(t)$, $V(t)$ and $V_{ph}(t)$ for $V_{DC} = -14$ kV and $V_{AC} = 12.8$ kV. Current scale 6 mA/div; voltage scale 5 kV/div, time scale 25 μs/div. (*a*) pmt at position A and (*b*) pmt at position B.

discharge with the presence of multiple short spikes appearing in both positive and negative cycles, which are closely related to corresponding light spikes registered by the phototube. However, the amplitude of the current spikes corresponding to the positive cycle of $I(t)$ was much larger than that corresponding to the negative cycle. The presence of spikes indicated that the discharge had a filamentary nature. On the other hand, it can be seen from figure 5(*b*) that the light pulses appearing during the positive cycle in $V_{ph}(t)$ are distributed on a time period shorter than that registered in $I(t)$ or $V_{ph}(t)$ at position A (see figure 5(*a*)) while there are no pulses in $V_{ph}(t)$ corresponding to the negative cycle at position B. Since the current pulses were detected independently of the space location of the phototube, this last result indicated that not all the filaments generated during the positive cycle were crossing the inter-electrode gap, but some of them remained 'anchored' between electrodes 1 and 3 (as in the purely SDBD) and hence they were not sensed by the phototube at position B. On the other hand, the current spikes corresponding to the negative cycle did not cross the gap between electrodes 1 and 2.

To derive some meaningful information on the discharge characteristics in terms of the V_{DC} and V_{AC} values, the following procedure was adopted. By setting the oscilloscope in the average acquisition mode an average waveform of the current signal over 128 samples was acquired. Then, to ignore the reactive component of the current (present even without the discharge), this statistical-averaged signal was

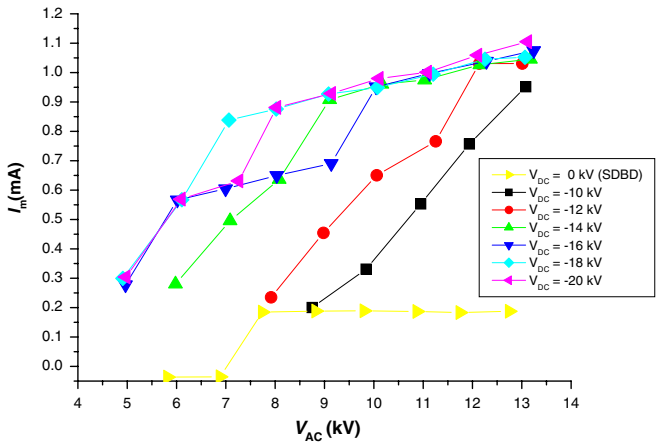

Figure 6. I_m versus V_{AC} for different V_{DC} values. The solid lines are only a guide for the eye.

time averaged over one period of the AC voltage to finally obtain an average current value of I_m. According to this described procedure the uncertainty in the I_m value could be estimated to be 0.1 mA.

The other important feature that characterized the sliding discharge behaviour was the amount of spikes generated during the discharge. This amount was represented by an averaged frequency that was obtained directly from the trigger frequency of the oscilloscope. For practical reasons, the $V_{ph}(t)$ waveform was selected to obtain the frequency, because in the current signal the spikes were superimposed to the alternating reactive current component, resulting in an ill-defined frequency value. Since this frequency fluctuated somewhat in time (the spikes were not purely periodic), we registered several frequency values of the oscilloscope (around 20 values) during a large time interval ($\sim$100 s) and finally calculated the statistical average value (f_s). The associated statistical uncertainties in f_s were not larger than 20%. It is important to mention that the f_s value depended on the selected amplitude of the spikes, which in turn were controlled by the trigger level of the oscilloscope. We thus decided to select a medium-amplitude trigger level, so as to register most of the spikes produced, but rejecting low-amplitude spikes that could be confused with the electrical noise of the discharge.

In figure 6 I_m as a function of V_{AC} with V_{DC} as a parameter is presented. Note that the sliding and the SDBD regimes are included in the plot. It can be seen from figure 6 that the I_m values associated with the pure SDBD case are very small as compared with the current values associated with the sliding discharge. The steep transition in I_m for $V_{AC} \sim 7.5$ kV for the SDBD case cannot be taken with confidence because the current amplitude variation at the transition was comparable to the measurement uncertainty (in fact, the behaviour of I_m could be a soft monotonic increase with V_{AC}, which has been masked by the large uncertainty). In the well-developed sliding discharge regime, and for a given value of V_{DC}, figure 6 indicates a marked increase in I_m with V_{AC}, up to a V_{AC} value where that marked increase in I_m is replaced by a smooth increase. The current values corresponding to the SDBD ($V_{DC} = 0$ kV) are also included in the figure.

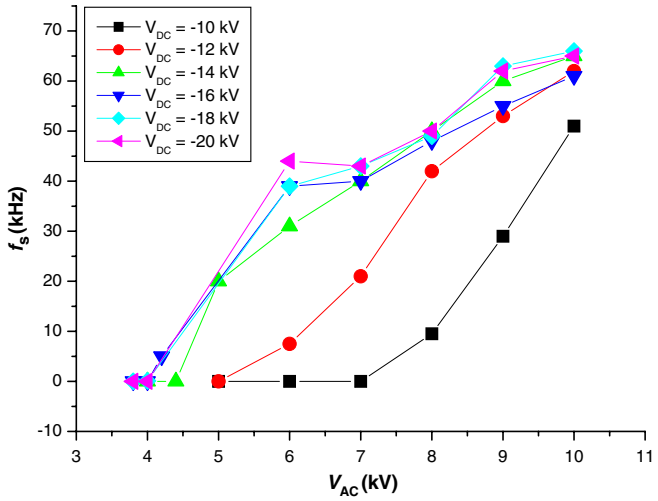

Figure 7. f_s versus V_{AC} for different V_{DC} values. The solid lines are only a guide for the eye.

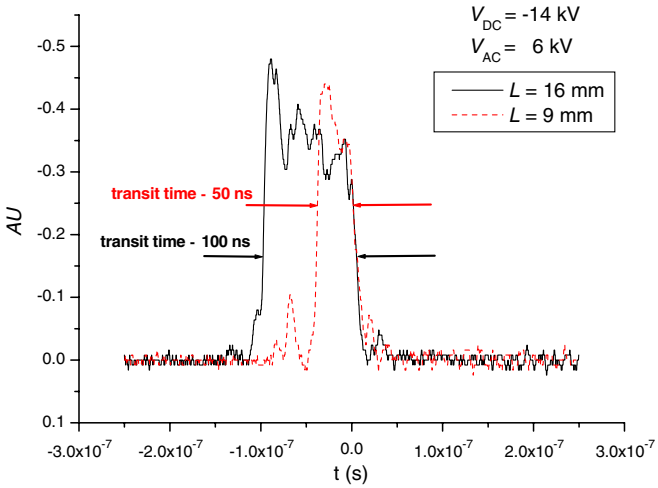

Figure 8. Waveforms of pmt signals (in arbitrary units, AU) corresponding to two different sizes of the field of view (rectangles with 16 mm × 3 mm and 9 mm × 3 mm in the x and z directions, respectively). $V_{DC} = -14$ kV and $V_{AC} = 6$ kV.

In figure 7 f_s as a function of V_{AC} with V_{DC} as a parameter is presented. The optical system was located at position B. Note first that the range of variation in V_{AC} is somewhat reduced with respect to that shown in the previous figure. This was due to the presence of the grounded holder of the phototube, which produced some sparking for high V_{AC} values. In any case, this restriction did not affect the general behaviour of the f_s curves. In general, it can be seen that the behaviour of f_s with V_{AC} (for a given V_{DC} value) is quite similar to that of I_m, showing again a strong increase with V_{AC} followed by a smooth increase.

In order to gain some information on the filament propagation velocity along electrodes 1 and 2, we used the described optical system but limiting its field of view to rectangles with dimensions of 16 mm × 3 mm and 9 mm × 3 mm in the x and z directions, respectively. This was done by using appropriate slits covering the converging lens. As a typical example, in figure 8 two $V_{ph}(t)$ waveforms (with a largely expanded time scale) are presented corresponding to both slits and for $V_{DC} = -14$ kV and $V_{AC} = 6$ kV. Assuming that the electron density profile that originates the light signal is steep, and that its longitudinal length is very short as compared with the slit sizes in the x direction (this is confirmed by the sharp rise and fall times of the light signals of figure 8), the transit time of the filament will be given simply by the temporal width of the light signal. Since the signal temporal widths increase approximately with the slit length in the x direction (∼50 ns and 100 ns, respectively), both transit times give an average velocity of $(2 \pm 0.4) \times 10^7$ cm s^{-1}. The longer signal presents some additional secondary spikes that could be due to a filament branching which is detected by the larger rectangle. A statistical analysis performed over several signals obtained under the whole range of V_{DC} and V_{AC} values leading to the sliding discharge regime showed an almost constant value for the filament velocity. Although several authors have reported a certain dependence of the filament velocity with the drop in electrodes' voltage [9, 10], the limited range of V_{DC} and V_{AC} values of this discharge together with the relatively large experimental uncertainty of the measurements (mainly due to discharge fluctuations) cannot be currently determined.

We also employed the optical system (but with a limited field of view) to investigate the spatial filament distribution along the z direction. In this case the slits were rotated by 90° (with their main length in the longitudinal direction) and the filament frequency was registered in different z positions and for different slit lengths. It was found that the registered frequency was proportional to the slit length, and independent of the z position, indicating that the filament distribution was almost uniform (within the uncertainty in the frequency measurement) along the electrodes' longitudinal length.

The emission lines were registered for practically all combinations between the V_{DC} and V_{AC} values leading to well-developed sliding discharges. Typical spectra corresponding to the FNS and to the SPS molecular nitrogen systems are presented in figure 9 (with an OMA acquisition time of 2 s).

Note the large difference in the amplitude of both lines. It was found that both FNS and SPS emissions were almost independent of the V_{DC} value and that both emissions increased monotonically with the V_{AC} value (with a similar behaviour as that shown for I_m and f_s in figures 6 and 7), but resulting in an almost constant intensity ratio value. A statistical analysis performed over more than twenty spectra showed that this line amplitude ratio between the FNS and SPS amplitudes was 0.02 ± 0.002.

4. Discussion of the results

Figure 3 given in section 3 is useful from a practical point of view because it defines the operating range of AC and DC voltage values to obtain a quasi-steady sliding discharge. The constancy of the V_{onset} value seems to be related to the presence of a minimum average electric field necessary for the filament propagation across the gap. The obtained value for this electric threshold value (∼6.3 kV cm^{-1}) is somewhat higher than other reported values (∼3–5 kV cm^{-1}) [12] but it must be taken into account that the actual $V(t)$ value for the filament propagation is smaller than its AC peak value (see figure 5(*b*)). This indicates the presence of remnant charged

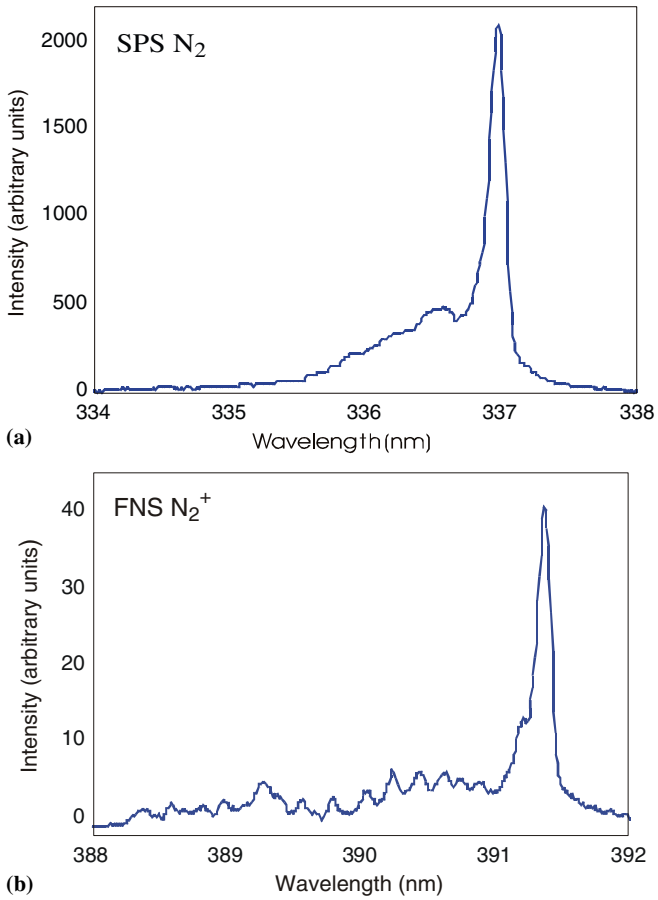

Figure 9. Typical nitrogen spectra of the sliding discharge. OMA acquisition time: 2 s. (*a*) SPS of nitrogen neutral molecule and (*b*) FNS of nitrogen molecular ion.

particles in the gap left during a given discharge cycle which favour the gas breakdown during the subsequent cycle (as it happens in pure dielectric barrier discharges [11]).

Concerning figures 6 and 7, the similar behaviour of I_m and f_s as functions of V_{AC} is remarkable. This fact, together with the similar behaviour of the spectral line amplitudes quoted at the end of section 3, suggests that the increase in I_m with V_{AC} is not associated with an increase in the amplitude of the individual spikes, but with an increase in their frequency. Currently, we do not have a clear explanation for the two different regimes appearing in these curves (with different slopes) but the smooth increasing stage might be related to external limitations in the electric circuit due to a limiting power (10 W) of our DC power source.

Several values of the physical quantities in the quasi-steady sliding discharge can be estimated from the optical emission spectroscopy measurements, together with a reliable atomic model to interpret the line emission from the discharge and employing the f_s values obtained in this work.

Following the work of Shcherbakov and Sigmond [13], it is possible to infer the number density of the excited emitting nitrogen species in terms of the number density of the neutral nitrogen molecule and the excitation rate (by electron impact) and quenching frequency (by both collisional de-excitation and spontaneous radiative decay) of the excited species. The intensity ratio corresponding to the maximum of the corresponding vibrational band heads (0–0 transition for the FNS of N_2^+ and SPS of N_2) is proportional to the respective ratio of the excited numerical species' densities and hence to the ratio between the corresponding excitation and quenching rates. Since these coefficients are functions of the reduced electric field E/N [13] (where E is the electric field value and N the number density of the air molecules), the value of this last parameter can be obtained from the experimentally determined line amplitude ratio. For an acquisition time of the OMA detector of 2 s, the line amplitude ratio was 0.02 ± 0.002, resulting in a value $E/N = (5 \pm 1) \times 10^{-15}\,\mathrm{V\,cm^{-2}} = 500 \pm 100\,\mathrm{Td}$ [14]. Taking the air number density corresponding to normal conditions ($N = 2.4 \times 10^{19}\,\mathrm{cm^{-3}}$), the resulting value for the electric field is $E = 120\,\mathrm{kV\,cm^{-1}}$. Although this value could be slightly modified by some gas heating by the discharge, such a high E value can be found under our experimental conditions only at the head of a streamer. Thus, the filaments previously mentioned in section 3 can be identified as streamers.

Once the E/N value is determined, the plasma density can be obtained using again the atomic model of Shcherbakov and Sigmond [13] with some additional assumptions. To this end, we have chosen the absolute value of the 391.4 nm emission line of N_2^+. This line was selected because of its optical transparency between the emission region and the detector. Following the quoted work, the continuity equation for the number density (N_2^{+*}) of excited states of the nitrogen molecular ion emitting the 391.4 nm line can be written as

$$\frac{\mathrm{d}(N_2^{+*})}{\mathrm{d}t} = k \cdot N_e \cdot N_2 - \nu \cdot N_2^{+*}, \tag{1}$$

where N_e and N_2 are the number densities of electrons and molecular nitrogen, respectively, and k and ν are the corresponding excitation rate and quenching frequency for the excited state of the nitrogen ion. Assuming equilibrium conditions, equation (1) allows expressing the excited number density in terms of the electron and molecular nitrogen densities. If additionally one considers an arbitrary volume, the total number of excited ion nitrogen molecules contained in such a volume (η^*) can be expressed in terms of the total electron number (η_e) and nitrogen molecules' density number N_2 as

$$\eta^* = \left(\frac{k}{\nu}\right) \eta_e N_2. \tag{2}$$

On the other hand, the energy (ε) radiated at 391.4 nm from the excited particles contained in such an arbitrary volume during a time t_{rad} which is being collected by a detector subtending a solid angle Ω can be written as (assuming optical transparency)

$$\varepsilon = t_{rad} \cdot \eta^* \cdot A_{ij} \cdot \varepsilon_f \cdot \left(\frac{\Omega}{4\pi}\right), \tag{3}$$

where A_{ij} is the spontaneous radiation probability of the line ($A_{ij} = 1.22\ 10^7\ \mathrm{s^{-1}}$) and ε_f is the photon energy ($\varepsilon_f = 3.7\,\mathrm{eV}$). The solid angle subtended by the detector can be expressed in this case in terms of the radius of the optical fibre (r_{of}) that sends the plasma light to the monochromator and the focal

distance (F) of the converging lens that focalizes the plasma light onto the optical fibre as

$$\Omega = 2 \cdot \frac{r_{\mathrm{of}}}{F}. \tag{4}$$

The energy ε collected by the detector can be related to the detector counts (C) experimentally obtained from the OMA output using the absolute detector sensitivity as

$$\varepsilon = S \cdot C \tag{5}$$

Finally, taking into account that the emitting object in this case is actually a succession of streamer heads crossing the vision field of the detector with frequency f_{s}, with a streamer transit time t_{t} along the light collecting region and with a certain acquisition detection time (t_{m}), the effective radiation time t_{rad} used in equation (3) can be expressed as

$$t_{\mathrm{rad}} = t_{\mathrm{t}} \cdot f_{\mathrm{s}} \cdot t_{\mathrm{m}}. \tag{6}$$

Equations (3)–(6) can be combined to express the total electron number contained in the emitting object (the streamer head) in terms of the detector counts, the streamer frequency, the streamer transit time and the other experimental and atomic parameters of the problem:

$$\eta_{\mathrm{e}} = \left(\frac{2\pi \cdot S \cdot F \cdot \nu}{t_{\mathrm{m}} \cdot r_{\mathrm{of}} \cdot A_{ij} \cdot \varepsilon_{\mathrm{f}} \cdot N_2 \cdot k} \right) \cdot \frac{C}{t_{\mathrm{t}} \cdot f_{\mathrm{s}}}. \tag{7}$$

Replacing in equation (7) the values of the parameters and taking $C \approx 40$, $t_{\mathrm{t}} \approx 10^{-7}$ s and $f_{\mathrm{s}} \approx 50$ kHz, it results in $\eta_{\mathrm{e}} = 5 \times 10^8$, which is a typical reported value for the total electron content in a streamer head [12, 15].

From the point of view of gas processing applications, it is interesting to derive time-averaged electron density values $\langle N_{\mathrm{e}} \rangle$ for the plasma generated by the sliding discharge. As the discharge is mainly constituted of streamers, we will consider only the streamer head, since it is well known [16] that most of the chemical species are produced mainly in that region of high electric field. One has to consider that the electrons are distributed in an effective volume equal to the discharge area in the x–z direction times the diameter of the streamer head in the y direction, and thus $\langle N_{\mathrm{e}} \rangle$ can be evaluated by first estimating the streamer head density N_{e} using the obtained value of η_{e} ($\eta_{\mathrm{e}} = 5 \times 10^8$) and assuming a certain size of the head (r_{h}). Since there is considerable dispersion in the reported value of r_{h} [17–20], we have taken a medium value ($r_{\mathrm{h}} = 0.1$ mm) for the calculation of N_{e}, resulting in $N_{\mathrm{e}} = 1.2 \times 10^{14}\,\mathrm{cm}^{-3}$. But it must be taken into account that the transit time of the streamer along the inter-electrode gap is very short ($\approx 10^{-7}$ s), while the streamer frequency is $f_{\mathrm{s}} \approx 50$ kHz (measured over a longitudinal size (D) of 2 cm), meaning that if one looks at a given point in the space, most of the time this space will be void. Actually, the time fraction that the streamer head occupies a certain spatial point is given by $t_{\mathrm{th}} \cdot f_{\mathrm{s}} \cdot (r_{\mathrm{h}}/D)$ where t_{th} is the transit time of the streamer along a distance equal to its own size. In our case this fraction amounts to 1.25×10^{-7}, thus giving $\langle N_{\mathrm{e}} \rangle = t_{\mathrm{th}} \cdot f_{\mathrm{s}} \cdot (r_{\mathrm{h}}/D) \cdot N_{\mathrm{e}} = 1.5 \times 10^7\,\mathrm{cm}^{-3}$.

Using the obtained value for the electric field, it is possible to estimate the average value of the electron temperature (T_{e}) under the assumption that the electrons have enough time to reach an equilibrium value of its mean energy in the presence of the electric field. Even with this simplifying assumption, the T_{e} value strongly depends on the electron energy loss (in elastic and inelastic collisions) to the neutral particles, so we have resorted to a software package [21] for the numerical solution of the Boltzmann equation for electrons in weakly ionized gases and in steady-state, uniform electric fields. Using air at atmospheric pressure and $E = 120\,\mathrm{kV\,cm}^{-1}$, $T_{\mathrm{e}} = 9$ eV is obtained.

5. Final remarks

By combining a surface dielectric barrier AC discharge together with a negative DC corona discharge at atmospheric pressure, a sliding discharge is generated. The ionization region of this discharge is considerably extended on the inter-electrode gap with respect to that usually obtained with a pure SDBD (which is mainly concentrated in the vicinity of electrode 1) and also with respect to the pure DC corona discharge (which is primarily concentrated in the vicinity of electrode 2). To our knowledge, previous work using a three-electrode geometry and combining AC and DC power sources can be found only in [22], but without performing a systematic plasma characterization of the discharge. Within a certain range of AC and DC voltage values, the discharge is quite stable and can be sustained over large times without any noticeable change in their average characteristics. It was found that the discharge is composed of repetitive streamers that are uniformly distributed along the whole electrode length and that propagate along the inter-electrode gap with an average velocity of $\sim 2 \times 10^7\,\mathrm{cm\,s}^{-1}$, and with an average electric field of $\sim 120\,\mathrm{kV\,cm}^{-1}$ and a total particle number of $\sim 5 \times 10^8$ at the streamer head. Assuming that the electron distribution function reaches an equilibrium value with the electric field, an electron temperature of 9 eV at the streamer head is obtained. The streamer frequency is around 5×10^4 Hz for a well-developed sliding discharge regime, and the time-averaged electron density amounts to $1.5 \times 10^7\,\mathrm{cm}^{-3}$.

References

[1] Kogelschatz U, Eliasson B and Egli W 1999 *Pure Appl. Chem.* **71** 1819–28

[2] Beverly R E III 1986 *J. Appl. Phys.* **60** 104–24

[3] Artana G, Sosa R, Moreau E and Touchard G 2003 Control of the near-wake flow around a circular cylinder with electrohydrodynamic actuators *Exp. Fluids* **35** 580–8

[4] Sosa R, Artana G, Moreau E and Touchard G 2007 Stall control at high angle of attack with plasma sheet actuators *Exp. Fluids* **42** 143–67

[5] Sosa R, Arnaud E and Artana G 2006 Study of the flow induced by a sliding discharge *Proc. Int. Symp. on Electrohydrodonamics (ISEHD)* (Buenos Aires, Argentina, 4–6 December 2006) pp 83–86 (ISBN 950-29-0964-X)

[6] Moreau E 2006 Airflow control by non-thermal plasma actuators *J. Phys. D: Appl. Phys.* **39** 1–32

[7] Kogelschatz U 2002 *IEEE Trans. Plasma Sci* **30** 1400–8
[8] Manish Y 2005 Pitot tube and wind tunnel studies of the flow induced by one atmosphere uniform glow discharge (oaugdp®) plasma actuators using a conventional and an economical high voltage power supply *MS Thesis* Department of Physics, University of Tennessee
[9] Akyuz M, Gao L, Larsson A, Cooray V, Gustavsson T G and Gubanski S M 2001 Positive streamer discharges along insulating surfaces *IEEE Trans. Dielectr. Electr. Insul.* **8** 902–10
[10] Yi W J and Williams P F 2002 Experimental study of streamers in pure N_2 and N_2/O_2 mixtures and a ≈13 cm gap *J. Phys. D: Appl. Phys.* **35** 205–18
[11] Gibalov V I and Pietsch G J 2000 The development of dielectric barrier discharges in gas gaps and on surfaces *J. Phys. D: Appl. Phys.* **33** 2618–36
[12] Raizer Y 1991 *Gas Discharge Physics* (Berlin: Springer)
[13] Shcherbakov Y V and Sigmond R S 2006 Novel high-resolved experimental results by sub-nanosecond spectral diagnostics of streamer discharges *Proc. 37th AIAA PDL Conf. (San Francisco, USA)* AIAA-2006-3758
[14] Lago V, Grondona D, Kelly H, Sosa R, Márquez A and Artana G 2006 Sliding discharge characteristics *Proc. Int. Symp. Electrohydrodonamics (ISEHD) (Buenos Aires, Argentina, 4–6 December 2006)* pp 87–90 (ISBN 950-29-0964-X)
[15] Fridman A, Chirokov A and Gutsol A 2005 Non-thermal atmospheric pressure discharges *J. Phys. D: Appl. Phys.* **38** R1–24
[16] Pancheshnyi S, Nudnova M and Starikovskii A 2005 Development of a cathode-directed streamer discharge in air at different pressures: experiment and comparison with direct numerical simulation *Phys. Rev.* E **71** 016407
[17] Morrow R and Lowke J J 1997 Streamer propagation in air *J. Phys. D: Appl. Phys.* **30** 614–27
[18] Pancheshnyi S V and Starikovskii Yu 2003 Two-dimensional numerical modeling of the cathode-directed streamer developement in a long gap at high voltage *J. Phys. D: Appl. Phys.* **36** 2683–91
[19] Shcherbakov Yu V, Shilova A V and Syssoev V S 1999 The near-surface evolution of streamer discharges *Electrical Insulation and Dielectric Phenomena (CEIDP) Conf. Annual Report (Austin, TX, 17–20 October 1999)* vol 2 pp 662–5
[20] Zhukov S V, Sokolova M V and Temnikov A G 2000 *Proc. 7th Int. Symp. on High Pressure Low Temperature Plasma Chemistry (Greifswald, Germany)*
[21] BOLSIG: CPAT & Kinema Software, http://www.siglo-kinema.com/bolsig.htm
[22] Louste C, Artana G, Moreau E and Touchard G 2005 Sliding discharge in air at atmospheric pressure: electrical properties *J. Electrostat.* **63** 615–20